

# The Space Density of Compton-thick AGN

Ezequiel Treister<sup>\*</sup>, Meg Urry<sup>†</sup>, Carolin Cardamone<sup>†</sup>, Shanil Virani<sup>†</sup>, Kevin Schawinski<sup>†</sup> and Eric Gawiser<sup>\*\*</sup>

<sup>\*</sup>*Institute for Astronomy, University of Hawaii*

<sup>†</sup>*Yale University*

<sup>\*\*</sup>*Rutgers University*

**Abstract.** We constrain the number density and evolution of Compton-thick Active Galactic Nuclei (AGN), and their contribution to the extragalactic X-ray background. In the local Universe we use the wide area surveys from the *Swift* and *INTEGRAL* satellites, while for high redshifts we explore candidate selections based on mid-IR parameters. We present the properties of a sample of 211 heavily-obscured AGN candidates in the Extended *Chandra* Deep Field-South (ECDF-S) selecting objects with  $f_{24\mu\text{m}}/f_R > 1000$  and  $R-K > 4.5$ . The X-ray to mid-IR ratios for these sources are significantly larger than that of star-forming galaxies and  $\sim 2$  orders of magnitude smaller than for the general AGN population, suggesting column densities of  $N_H > 5 \times 10^{24} \text{ cm}^{-2}$ . The space density of CT AGN at  $z \sim 2$  derived from these observations is  $\sim 10^{-5} \text{ Mpc}^{-3}$ , finding a strong evolution in the number of  $L_X > 10^{44} \text{ erg/s}$  sources from  $z = 1.5$  to  $2.5$ .

**Keywords:** galaxies: active, Seyfert. X-rays: diffuse background

**PACS:** 98.54.Cm, 98.70.Vc, 98.62.Js

## COMPTON THICK AGN WITH INTEGRAL AND SWIFT

The most obscured AGN known are those in which the neutral hydrogen column density ( $N_H$ ) in the line of sight is higher than the inverse Thomson cross section,  $N_H \simeq 1.5 \times 10^{24} \text{ cm}^{-2}$ . These are the so-called Compton-thick (CT) AGN. Contrary to the situation for less obscured sources, not much is known about the number density of CT AGN. Thanks to the deep *Chandra* and *XMM-Newton* surveys it is now clear that the fraction of moderately obscured, Compton-thin, AGN is on average  $\sim 3/4$  of all AGN, and is higher at lower luminosities [1, 2] and higher redshifts [3], but there are no comparable constraints on the number of CT AGN. One of the best ways to find CT AGN is by observing at high energies, namely  $E > 10 \text{ keV}$ . One clear advantage of these high-energy observations is that photoelectric absorption has minimal effects, so even CT AGN can be easily detected.

Using the IBIS coded-mask telescope, *INTEGRAL* surveyed  $\sim 80\%$  of the sky down to a flux of 5 mCrab in the 17-60 keV band. The catalog of Krivonos et al. [4] reports the properties of 130 sources detected in these all-sky observations and classified as AGN. Five of the 130 AGN are CT AGN. Similarly, Tueller et al. [5] presented a catalog of 103 AGN detected in an all-sky survey with the *Swift/BAT* telescope. Excluding blazars, BL Lac and low galactic latitude observations, we obtained a sample of 89 sources, where only one source remains unidentified. In the Tueller et al. [5] catalog there are five AGN with estimated  $N_H$  greater than  $10^{24} \text{ cm}^{-2}$ . Figure 1 shows the cumulative number counts of AGN, with CT sources shown separately, as a function of hard X-ray flux. In order

to avoid the necessity of specifying a standard spectrum to convert fluxes to different energy bands, we show the *INTEGRAL* and *Swift* sources separately, but note that a good agreement (within  $\sim 40\%$ ) in the normalization between the two distributions exist if a standard band conversion is assumed. At these high fluxes the slope of the log N-log S is Euclidean, implying an uniform spatial distribution, as expected given the low redshifts of these sources. We also compare with the distribution predicted by the AGN population synthesis model with which Treister and Urry [2] fit the XRB, and find in general good agreement in slope and normalization.

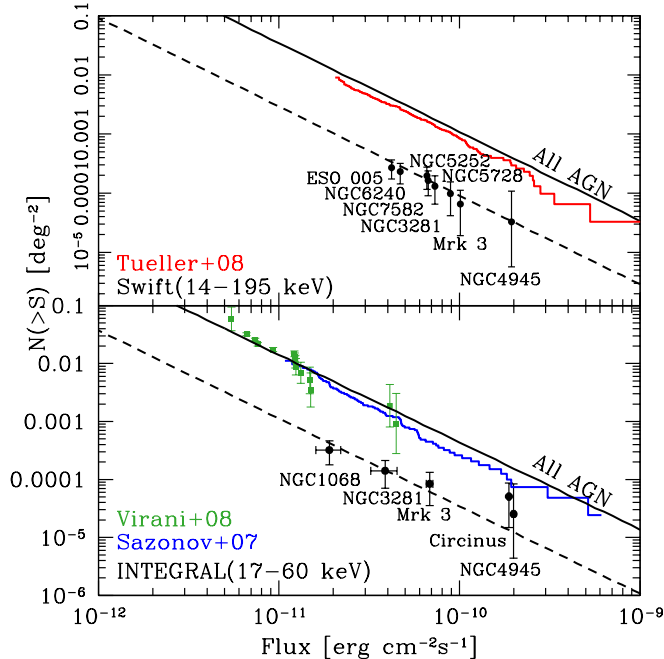


**FIGURE 1.** LogN-logS distribution for AGN detected at high energies. The *red line* shows the AGN in the well-defined *Swift/BAT* samples in the 14-195 keV band [5], while the *bottom panel* shows the *INTEGRAL* sources [4] in the 17-60 keV band. *Solid squares* show the 14 sources detected in the deep 3 Msec *INTEGRAL* observations of the *XMM-LSS* field (S. Virani in prep.). *Solid circles* mark the CT AGN detected with *Swift* (*top panel*) and *INTEGRAL* (*bottom panel*). The *black solid lines* shows the expected AGN logN-logS from the population synthesis model of Treister and Urry [2], which at these fluxes corresponds to a Euclidean distribution. The *dashed lines* mark the Euclidean slope normalized to the number of *Swift* and *INTEGRAL* CT AGN.

Since now the number density of CT AGN can be constrained independently, we can attempt to match the observed spectrum and intensity of the X-ray background (XRB). In Figure 2, we show our new fit, which matches the both the *INTEGRAL* and *Swift/BAT* observations at  $E > 10$  keV and the *Chandra* measurements at lower energies (which are  $\sim 30\%$  higher than the *HEAO-1* A2 observations). These new data confirmed that the original *HEAO-1* normalization should be increased by  $\sim 30\%$  and  $\sim 10\%$  at low and high energies respectively. In contrast, the AGN population synthesis model of Gilli et al. [6] assumed the original *HEAO-1* intensity at all energies, which translates into a relatively lower contribution from unobscured sources. In order to produce the necessary hard spectrum, Gilli et al. [6] had to assume a relatively high number of obscured sources at high luminosities, i.e., an unusual, inverted dependence of the obscured fraction of AGN as a function of luminosity [7].

## IR SELECTION OF HIGH- $z$ CT AGN

Because most of the radiation absorbed at X-ray and UV wavelengths is then re-emitted in the mid- and far-IR, recent studies at these energies, mostly taking advantage of

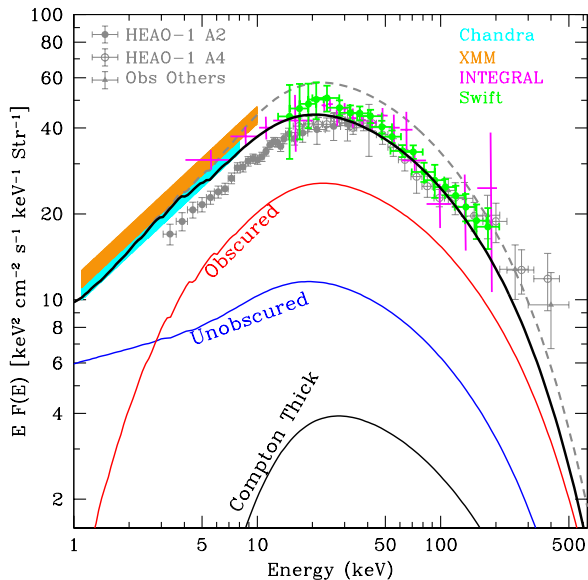


**FIGURE 2.** Observed spectrum of the extragalactic X-ray background from *HEAO-1* [8], *Chandra* [9], *XMM* [10], *INTEGRAL* [11] and *Swift* [12] data. The *dashed gray line* shows the XRB spectrum from the AGN population synthesis model of Treister and Urry [2], which assumed a 40% higher value for the *HEAO-1* XRB normalization. The *thick black solid line* shows our new population synthesis model for the XRB spectrum; the only change is the number of CT AGN, which is reduced by a factor of 4 relative to the number in Treister and Urry [2]. *Red, blue and thin black solid lines* show the contribution to this model from unobscured, obscured Compton thin and CT AGN respectively.

*Spitzer* observations, have been very successful in finding heavily-obscured AGN candidates missed by X-ray selection up to high redshifts. In particular, Fiore et al. [13] presented a selection method based on the  $24 \mu\text{m}$  to R band flux ratio and  $R-K$  color; specifically,  $f_{24}/f_R > 1000$  and  $R-K > 4.5$  (Vega). According to simulations based on stacking of the X-ray signal, they estimate the fraction of heavily-obscured AGN in this sample to be greater than 80%. We applied this selection criteria to the MIPS-selected sources in the ECDF-S to select CT AGN candidates. Of the 7201  $24\mu\text{m}$  sources detected to a flux limit of  $\sim 35 \mu\text{Jy}$ , 211 ( $\sim 3\%$ ) satisfy the  $f_{24}/f_R > 1000$  and  $R-K > 4.5$  cuts. Of the 651 X-ray detected sources in the Virani et al. [14] catalog, 18 are found in this region,  $\sim 2.8\%$ , a similar fraction as in the general population.

As can be seen in Fig. 3, the X-ray to mid-IR ratio for the IR-red excess sources is about two orders of magnitude smaller than the average value for the X-ray-detected sample and for most sources falls in the range expected for obscuration of  $\sim 5 \times 10^{24}$  to  $10^{25} \text{ cm}^{-2}$ . The observed ratio for the IR-red excess sample is significantly larger than for the sources outside our selection region, even at similar rest-frame  $12 \mu\text{m}$  luminosities. The observed X-ray to mid-IR ratio for IR-red excess sources at  $L_{12\mu\text{m}} \sim 10^{45} \text{ erg s}^{-1}$  is roughly 3-4 times larger than the values expected from the X-ray versus mid-IR luminosity for star-forming galaxies, thus confirming the AGN nature for the vast majority of our sample. The space density of CT AGN as a function of redshift inferred from these observations is shown in Fig. 3.

## ACKNOWLEDGMENTS

Support for the work of ET and KS was provided by NASA through *Chandra* Postdoctoral Fellowship Award Numbers PF8-90055 and PF9-00069 respectively issued by the *Chandra* X-ray Observatory Center, which is operated by the Smithsonian Astrophysical Observatory for and on behalf of NASA.

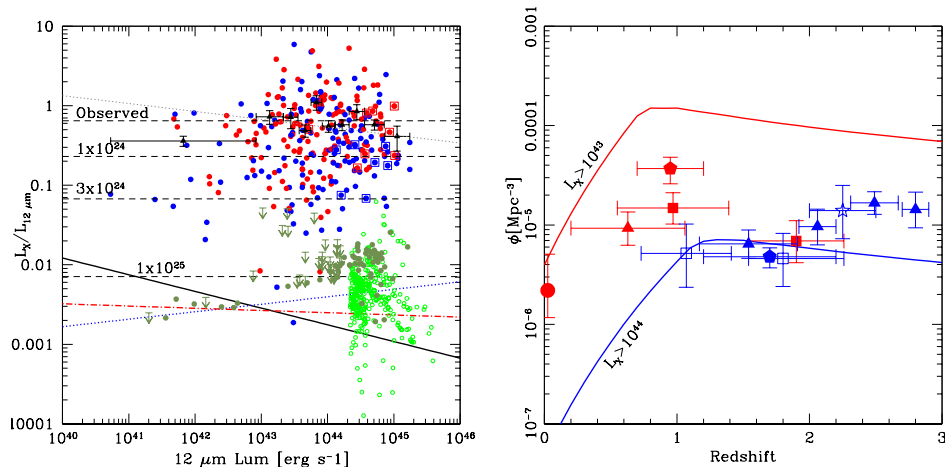


**FIGURE 3.** *Left panel:* Ratio of hard X-ray to mid-IR versus rest-frame  $12\ \mu m$  luminosity. *Red and blue circles* show the obscured and unobscured X-ray detected sources respectively. *Black triangles with error bars* show the average ratio for these sources. *Circles enclosed by squares* identify the X-ray detected IR-red excess sources. The *dashed line* at a ratio of  $\sim 0.6$  shows the average value of  $L_X/L_{12\mu m}$  for all the X-ray sources. The *dotted line* shows the relation between intrinsic X-ray and  $12\ \mu m$  luminosity for local Seyfert galaxies. *Green circles* show the location of the most luminous rest-frame  $12\ \mu m$  X-ray undetected sources outside the selection region. X-ray undetected IR-red excess sources are shown by olive circles and upper limits. *Dashed lines* show the effects of X-ray obscuration in the observed  $L_X/L_{12\mu m}$  ratio. The *thick solid, dot-dashed and dotted lines* show the expected  $L_X/L_{12\mu m}$  for star-forming galaxies, considering different recipes to convert star formation rates into X-ray and IR luminosities. *Right panel:* Space density of CT AGN as a function of redshift. Measurements obtained by Tozzi et al. [15], Alexander et al. [16], Fiore et al. [17] and this work are shown by *squares, stars, pentagons and triangles* respectively. *Solid lines* show the expected space density of CT AGN from the luminosity functions of Della Ceca et al. [18]. *Red and blue symbols* show measurements and expectations for  $L_X > 10^{43}$  and  $> 10^{44}$  erg s<sup>-1</sup> sources. These observations indicate a strong increase in the number of high-luminosity CT AGN at  $z > 2$ .

## REFERENCES

1. Y. Ueda, M. Akiyama, K. Ohta, and T. Miyaji, *ApJ* **598**, 886–908 (2003).
2. E. Treister, and C. M. Urry, *ApJ* **630**, 115–121 (2005).
3. E. Treister, and C. M. Urry, *ApJ* **652**, L79–L82 (2006).
4. R. Krivonos, M. Revnivtsev, A. Lutovinov, S. Sazonov, E. Churazov, and R. Sunyaev, *A&A* **475**, 775–784 (2007).
5. J. Tueller, et al., *ApJ* **681**, 113–127 (2008).
6. R. Gilli, A. Comastri, and G. Hasinger, *A&A* **463**, 79–96 (2007).
7. E. Treister, et al., *ApJ* **693**, 1713–1727 (2009).
8. D. E. Gruber, J. L. Matteson, L. E. Peterson, and G. V. Jung, *ApJ* **520**, 124–129 (1999).
9. R. C. Hickox, and M. Markevitch, *ApJ* **645**, 95–114 (2006).
10. A. De Luca, and S. Molendi, *A&A* **419**, 837–848 (2004).
11. E. Churazov, et al., *A&A* **467**, 529–540 (2007).
12. M. Ajello, et al., *ApJ* **689**, 666–677 (2008).
13. F. Fiore, et al., *ApJ* **672**, 94–101 (2008).
14. S. N. Virani, E. Treister, C. M. Urry, and E. Gawiser, *AJ* **131**, 2373–2382 (2006).
15. P. Tozzi, et al., *A&A* **451**, 457–474 (2006).
16. D. M. Alexander, et al., *ApJ* **687**, 835–847 (2008).
17. F. Fiore, et al., *ApJ* **693**, 447–462 (2009).
18. R. Della Ceca, et al., *A&A* **487**, 119–130 (2008).